

# A Myelin-Specific Contrast Agent for Magnetic Resonance Imaging of Myelination

Luca Frullano,<sup>†</sup> Changning Wang,<sup>†</sup> Robert H. Miller,<sup>‡</sup> and Yanming Wang<sup>\*,†</sup>

<sup>†</sup>Division of Radiopharmaceutical Science, Case Center for Imaging Research, Department of Radiology, and

<sup>‡</sup>Department of Neuroscience, Case Western Reserve University, Cleveland, Ohio 44106, United States

**S** Supporting Information

**ABSTRACT:** Myelination is one of the most fundamental biological processes in the development of vertebrate nervous systems. Abnormal or disrupted myelination occurs in many acquired or inherited neurodegenerative diseases, including multiple sclerosis (MS) and various leukodystrophies. To date, magnetic resonance imaging (MRI) has been the primary tool for diagnosing and monitoring the progression of MS and related diseases; however, any change in signal intensity of conventional MRI reflects a change only in tissue water content, which is a nonspecific measure of the overall changes in macroscopic tissue injury. Thus, the use of MRI as a primary measure of disease activity was shown to be disassociated from the clinical outcome due to the lack of specificity for myelination. In order to increase the MRI specificity for myelin pathologies, we designed and synthesized the first Gd-based T<sub>1</sub> MR contrast agent (MIC) that binds to myelin with high specificity. In this Communication, we demonstrate that MIC localizes in brain regions in proportion to the extent of myelination. In addition, MIC possesses promising MR contrast properties, which allow for direct detection of myelin distribution through T<sub>1</sub> mapping in the mouse brain.

In this Communication, we report a myelin-specific Gd-based magnetic resonance contrast agent for imaging of myelination. Myelination is one of the most fundamental biological processes in nervous system development that defines the vertebrate species.<sup>1</sup> Myelin sheaths provide a unique structure in the nervous system that fosters rapid and efficient conduction of impulses along axons.<sup>2</sup> Abnormalities or destruction of myelin occur in many acquired or inherited neurodegenerative diseases, including multiple sclerosis (MS) and various leukodystrophies.<sup>3</sup> MS, which affects an estimated 350 000 people in the United States and 2 million people worldwide, is the most commonly acquired myelin disease in humans.<sup>4</sup> The leukodystrophies, on the other hand, are the result of inherited enzyme deficiencies that cause abnormal formation, destruction, and/or abnormal turnover of myelin sheaths within the central nervous system (CNS) white matter.<sup>5</sup> One major challenge has been assessing and quantifying changes in myelin content *in vivo*.

To date, magnetic resonance imaging (MRI) has been the primary tool for diagnosing and monitoring the progression of myelin diseases.<sup>6,7</sup> Unfortunately, any change in signal intensity on

a dual-echo T<sub>2</sub>-weighted sequence reflects a change in tissue water content, which is a nonspecific measure of the overall changes in macroscopic tissue injury ranging from edema to inflammation, demyelination, and axonal loss.<sup>8</sup> As a result, the use of MRI as a primary measure of disease activity still has not been accepted by the FDA, as it was shown to be dissociated from the clinical attack rate in disease-modifying therapies. This dissociation was evidenced by a clinical study of interferon- $\beta$  measured by conventional MRI parameters.<sup>9</sup> Although additional MRI techniques, such as magnetization transfer (MT)<sup>10</sup> and diffusion tensor imaging (DTI),<sup>11</sup> have been developed, use of these techniques still lacks specificity for more destructive myelin pathology.

Thus, a long-standing goal has been to develop a direct measure of myelination that will effectively correlate clinical outcomes with myelin changes. This requires the development of contrast agents for MR imaging of myelin. Recently, an attempt has been made to use Luxol Fast Blue (LFB), a histological stain for myelin with a paramagnetic copper core, as a MR probe.<sup>12</sup> However, LFB shows low relaxivity ( $r_1 = 0.09 \text{ s}^{-1} \text{ mM}^{-1}$ , room temperature, 4.7 and 14 T), modest solubility, and limited tissue permeability and requires post-incubation tissue processing to differentiate myelinated regions.

For this reason, we set out to develop a small-molecule MR contrast agent that is myelin specific with suitable MR-imaging properties that could potentially be applied *in vivo*. In this Communication, we report, for the first time, the design and synthesis of a Gd-based T<sub>1</sub> MR contrast agent that binds specifically to myelin membranes and demonstrate its efficacy to discriminate myelinated regions in mouse brains by MRI.

Over the past years, we have developed a wide array of small-molecule probes for myelin imaging. One of these imaging agents, termed CMC, readily enters the brain and selectively binds to myelinated fibers.<sup>13</sup> In addition, our ongoing studies have shown that the structure of CMC is amendable and methylation or alkylation of the amino group has no negative impact on its myelin-binding property. We thus hypothesized that the structure of CMC could be modified by conjugation with a Gd complex for MR imaging while preserving its ability to bind specifically to myelin. To test this hypothesis, we designed and synthesized MIC as shown in Scheme 1.

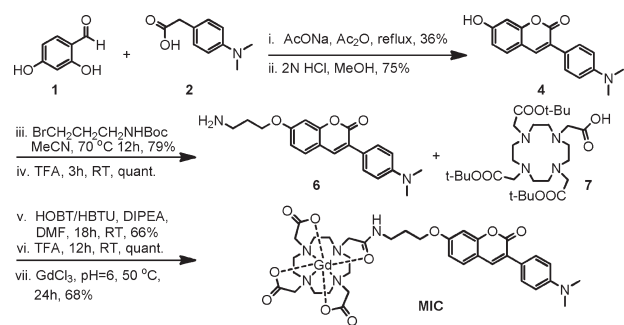
The coumarin derivative with a nucleophilic hydroxyl group (**4**) was prepared in two steps via a Perkin condensation of **1** and **2**, followed by hydrolysis. A three-carbon spacer was then introduced

**Received:** May 12, 2010

**Revised:** December 7, 2010

**Published:** January 25, 2011

### Scheme 1. Synthesis of MIC, a MR Contrast Agent for Myelin



by reacting **4** with Boc-protected 3-bromopropylamine. After deprotection, **6** was coupled with DOTA-*tert*-butyl ester (**7**). Treatment with neat trifluoroacetic acid yielded the deprotected ligand, which gave the myelin-targeting probe MIC upon complexation with  $\text{GdCl}_3$  in water.

MIC's longitudinal relaxivity ( $r_1 = 5.2 \text{ s}^{-1} \text{ mM}^{-1}$ ,  $21^\circ \text{C}$ ,  $9.4 \text{ T}$ ) is more than 50 times greater than that of LFB. At clinically relevant magnetic fields such as 1.41 and  $0.47 \text{ T}$ , MIC's longitudinal relaxivity ( $r_1$ ) at  $40^\circ \text{C}$  is 5.1 and  $5.8 \text{ s}^{-1} \text{ mM}^{-1}$ , respectively, which is ca. 1.5 times greater than those of commercial MR contrast agents such as Magnevist and Dotarem at the same magnetic fields.<sup>14</sup> The transmetalation stability of MIC toward Zn proved to be excellent and in line with other DOTA-monoamide complexes.<sup>15</sup>

MIC is a fluorescent compound with maximal excitation and emission at 460 and 570 nm, respectively. We thus examined the myelin-binding property of MIC by fluorescent staining of mouse brain tissue sections. For comparison, the same sections were then subjected to immunohistochemical staining for myelin basic protein (MBP), a distinctive protein that is characteristic of myelin membranes. Axial sections of the whole brain were used to examine myelin-binding properties of MIC in different brain regions, either rich or poor in myelin. As shown in Figure 1A,B, MIC staining (blue) is very similar to immunohistochemical staining (red). At a  $100 \mu\text{M}$  concentration, MIC selectively labeled myelinated fibers in myelin-rich white matter regions such as the cerebellum (Figure 1C), corpus callosum (Figure 1F), and striatum (Figure 1G). Subsequent immunohistochemical staining for MBP in the same regions (Figure 1B,D,I,J, respectively) allowed us to determine if MIC binds to myelin, oligodendrocytes, or both. From the data presented, we concluded that MIC selectively binds to myelin but not oligodendrocytes, which accounts for the small difference between MIC and immunohistochemical staining for MBP in the images shown below. For example, the myelin-deficient subcortical gray matter region showed little MIC staining (Figure 1E) but more MBP staining (Figure 1H). These studies demonstrate that MIC selectively binds to myelin present in the white matter regions, while MBP staining also labels oligodendrocyte cell soma and processes.

Based on the high binding specificity of MIC for myelin, the MR properties of MIC were then comprehensively evaluated in the brains of wild-type mice and C3Fe.SWV-Mbpshi/J shiverer mice, an autosomal recessive mutant with myelin deficiency in the CNS. After 24 h of incubation in 1.0 mM water solution of MIC ( $0.4 \text{ mL}$ ) followed by extensive washing with saline, the brain tissues were imaged by MR for both proton density weighted images and  $T_1$  mapping.

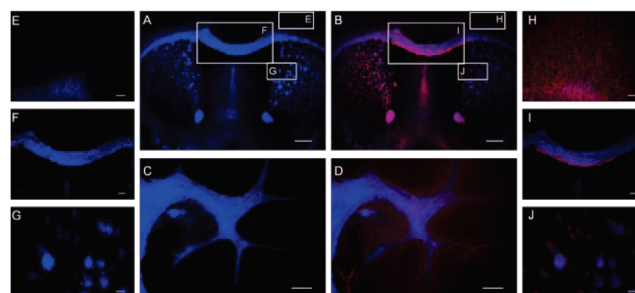


**Figure 1.** (A) MIC staining of the whole mouse brain tissue section *in vitro* and (B) subsequent immunohistochemical staining for MBP of the same section. (C) MIC staining of the cerebellum and (D) subsequent immunohistochemical staining for MBP of the same section. For clarity, the MIC staining and the subsequent MBP staining of the myelin-deficient subcortical gray matter region (E,H) and the myelin-rich corpus callosum (F,I) and striatum regions (G,J) are highlighted separately. Scale bar: A,B =  $500 \mu\text{m}$ , C,D,F,I =  $300 \mu\text{m}$ , E,H =  $100 \mu\text{m}$ , G,J =  $50 \mu\text{m}$ .

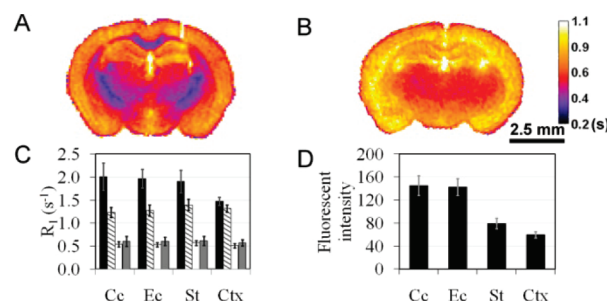


**Figure 2.** Representative MR  $T_1$  maps of wild-type (A) and shiverer (B) mouse brain tissues. (C) Average water proton relaxation rate in MIC-treated wild-type (black) and shiverer (dashed) mouse brains and untreated wild-type (white) and shiverer (gray) mouse brains ( $n = 3$ ). (D) Average fluorescent intensity of wild-type mouse brain sections treated with MIC ( $n = 5$ ). The error bars represent the standard error of the mean.

For MR imaging,  $T_1$  was measured at  $9.4 \text{ T}$  and room temperature using a multiple TR spin-echo acquisition ( $\text{TE } 7.0 \text{ ms}$ ,  $\text{TR } 100\text{--}2500 \text{ ms}$ ,  $0.098 \times 0.098 \text{ cm/pixel}$ , matrix size  $256 \times 256$ ), and  $T_1$  maps were generated using the QuickVol II plug-in in ImageJ (Figure 2A,B).<sup>16</sup> Prior to incubation with MIC,  $T_1$  maps were acquired in both wild-type and shiverer mouse brains. In MIC untreated brains, different regions could not be conspicuously distinguished in  $T_1$  maps. After incubation with MIC, contrast was observed in  $T_1$  maps of wild-type mouse brains in proportion to the myelin content. In the MIC-treated wild-type mouse brains, the longitudinal relaxation rates and fluorescent intensities in the myelinated white matter regions (i.e., corpus callosum and the external capsule) are significantly higher than those in the subcortical region ( $p < 0.05$ ) (Figure 2C,D). In the MIC-treated myelin-deficient shiverer mouse brains,  $T_1$  is more uniform throughout the brain. The  $T_1$  maps showed no statistical difference between the gray and white matter ( $p > 0.6$ ) within the same shiverer mouse brains. Compared to the wild-type mice,  $T_1$  of the shiverer mice is significantly longer in the white matter regions ( $p < 0.05$ ). Thus, the MR data suggest that retention of MIC is proportional to the level of myelination in the brain. Following the MR imaging studies, the stability of MIC in the incubated tissues was verified by HPLC analysis of extracts of the pulverized brain tissues.

In conclusion, we developed the first Gd-based MRI contrast agent that selectively localizes in myelinated brain regions and allows

for myelin mapping in MR images. The exact binding mechanism of MIC remains to be delineated. Such a MR contrast agent is expected to improve the specificity of MR imaging of myelination in both peripheral and central nervous systems. Further studies are under way to investigate the *in vivo* MR properties, biodistribution, and pharmacokinetics of MIC in animal models of myelin-related diseases.

## ■ ASSOCIATED CONTENT

**S Supporting Information.** Detailed experimental procedures, including synthetic methods, protocols for animal preparation, chemical and immunohistochemical staining protocols, and MR imaging procedures; statistical analysis of MIC distribution; analysis of MIC stability in incubated tissues; fluorescent imaging; MIC transmetalation stability; and relaxivity measurements. This material is available free of charge via the Internet at <http://pubs.acs.org>.

## ■ AUTHOR INFORMATION

**Corresponding Author**  
yanming.wang@case.edu

## ■ ACKNOWLEDGMENT

We gratefully acknowledge financial support from the Department of Defense (MS090082), National Multiple Sclerosis Society, and NIH/NINDS (R01 NS061837). We thank Dr. Christopher Flask for his advice and expertise on MR imaging protocols.

## ■ REFERENCES

- (1) Sherman, D. L.; Brophy, P. J. *Nat. Rev. Neurosci.* **2005**, *6*, 683–690.
- (2) Hildebrand, C.; Remahl, S.; Persson, H.; Bjartmar, C. *Prog. Neurobiol.* **1993**, *40*, 319–384.
- (3) Hauw, J. J.; Delaere, P.; Seilhean, D.; Cornu, P. *J. Neuroimmunol.* **1992**, *40*, 139–152.
- (4) Compston, A.; Coles, A. *Lancet* **2002**, *359*, 1221–1231.
- (5) Schiffmann, R.; Boespflug-Tanguy, O. *Curr. Opin. Neurol.* **2001**, *14*, 789–794.
- (6) Polman, C. H.; Reingold, S. C.; Edan, G.; Filippi, M.; Hartung, H.-P.; Kappos, L.; Lublin, F. D.; Metz Luanne, M.; McFarland, H. F.; O'Connor, P. W.; Sandberg-Wollheim, M.; Thompson, A. J.; Weinshenker, B. G.; Wolinsky, J. S. *Ann. Neurol.* **2005**, *58*, 840–846.
- (7) Polman, C. H.; Wolinsky, J. S.; Reingold, S. C. *Mult. Scler.* **2005**, *11*, 5–12.
- (8) Filippi, M.; Falini, A.; Arnold, D. L.; Fazekas, F.; Gonen, O.; Simon Jack, H.; Dousset, V.; Savoiardo, M.; Wolinsky, J. S. *J. Magn. Reson. Imaging* **2005**, *21*, 669–675.
- (9) Molyneux, P. D.; et al. *Neurology* **2001**, *57*, 2191–2197.
- (10) Le Bihan, D.; Mangin, J. F.; Poupon, C.; Clark, C. A.; Pappata, S.; Molko, N.; Chabriet, H. *J. Magn. Reson. Imaging* **2001**, *13*, 534–546.
- (11) Song, S.-K.; Sun, S.-W.; Ramsbottom, M. J.; Chang, C.; Russell, J.; Cross, A. H. *Neuroimage* **2002**, *17*, 1429–1436.
- (12) Blackwell, M. L.; Farrar, C. T.; Fischl, B.; Rosen, B. R. *Neuroimage* **2009**, *46*, 382–393.
- (13) Wang, C.; Popescu, D. C.; Wu, C.; Zhu, J.; Macklin, W.; Wang, Y. *J. Histochem. Cytochem.* **2010**, *58*, 611–621.
- (14) Rohrer, M.; Bauer, H.; Mintorovitch, J.; Requardt, M.; Weinmann, H.-J. *Invest. Radiol.* **2005**, *40*, 715–724.
- (15) Laurent, S.; Vander, L.; Copoix, F.; Muller, R. N. *Invest. Radiol.* **2001**, *36*, 115–122.
- (16) Schmidt, K. F.; Ziu, M.; Schmidt, N. O.; Vaghasia, P.; Cargioli, T. G.; Doshi, S.; Albert, M. S.; Black, P. M. L.; Carroll, R. S.; Sun, Y. *J. Neurooncol.* **2004**, *68*, 207–215.